ISA Transactions 129 (2022) 436–445

Contents lists available at ScienceDirect

ISA Transactions

journal homepage: www.elsevier.com/locate/isatrans

Practice article

Finite-time adaptive sliding mode control for high-precision tracking of piezo-actuated stages

Zhongshi Wang [a], Rui Xu [a], Lina Wang [b], Dapeng Tian [a,*]

[a] Key Laboratory of Airborne Optical Imaging and Measurement, Changchun Institute of Optics, Fine Mechanics and Physics, Chinese Academy of Sciences, Changchun 130033, China
[b] College of Electro-Mechanical Engineering, Changchun University of Science and Technology, Changchun 130022, China

ARTICLE INFO

Article history:
Received 5 August 2021
Received in revised form 4 December 2021
Accepted 4 December 2021
Available online 13 December 2021

Keywords:
Piezo-actuated stage
Dynamic hysteresis nonlinearity
Rate-dependent
Bouc–Wen model
Finite-time adaptive sliding mode control

ABSTRACT

Piezo-actuated stages are widely used in nanopositioning applications. However, they not only have inherent static hysteresis characteristics but also have dynamic rate-dependent hysteresis nonlinearity. Therefore, to address dynamic hysteresis nonlinearity and uncertainty in the model parameters, an adaptive switching-gain sliding mode controller with a proportional–integral–derivative surface is designed. In particular, the combination of Bouc–Wen model and second-order linear system is used to describe the dynamic hysteresis process. To improve the robustness and reduce chattering in the sliding mode control method, an adaptive switching-gain is added to the controller without knowing in advance the upper bound of uncertainties. Finite-time convergence conditions of the closed-loop system are also analyzed. Finally, the proposed control method is implemented in real time on an ARM experimental platform. Comparative experimental results demonstrate excellent tracking performance and robustness. The dynamic hysteresis characteristics are suppressed effectively, and this result provides a powerful reference for engineering applications.

1. Introduction

The piezo-actuated stage plays an important role in micromanipulators [1], laser communication [2,3], surgical devices [4], fast steering mirrors [5], and other devices because of its advantages of high precision, fast response, and large output force. However, a piezo-actuated stage has undesirable nonlinear behavior, which is its main limitation in positioning applications. The nonlinear behavior, specially the hysteresis, is a special memory-based nonlinear phenomenon between input voltage and output displacement. The behavior exhibits not only a static hysteresis loop but also dynamic rate-dependent characteristics, as illustrated in Fig. 1. This implies that, when the input control signal rate of the piezo-actuated stage is increased, the hysteresis loop becomes fatter and rounder. This characteristic not only induces errors in the system, but it also causes control difficulties because it is difficult to model and can even cause instability in the close-loop controller [6]. This issue has become the main challenge for high-precision tracking control of piezo-actuated stages [7]. Therefore, a control algorithm that is robust to dynamic hysteresis nonlinearity should be developed.

Proportional integral derivative (PID) control is a typical representative of model-free control methods. PID control is widely used in industrial piezoelectric ceramic controllers because of its good robustness and ability to tune parameters easily [8,9]. However, as the frequency of the input signal increases, the rate-dependent characteristic causes the signal phase to lag severely, causing the performance of the PID controller to decline sharply. To achieve high-precision tracking control, many methods based on an accurate hysteresis model have been proposed in the existing literature. The model-based approaches develop a more accurate mathematical model. Generally, the main hysteresis models for piezo-actuated stages are operator-based or differential-equation-based models [10]. At present, the Preisach model [11], Krasnosel'skii–Pokrovskii model [12], and Prandtl–Ishinskii model [13] are the most common operator-based models. However, operator-based models have many parameters and a large amount of calculation; hence, it is difficult to apply them in microprocessor chips. The differential-equation-based models, such as the Duhem model [14], Backlash-like model [15], and Bouc–Wen model [16], are described by a differential equation, which is closer to a linear system and more suitable for our study.

Based on these models, many controllers have been designed to compensate for the hysteresis nonlinearity and improve tracking performance in piezo-actuated stages. Some researchers have effectively reduced the effect of hysteresis using feedforward

* Corresponding author.
E-mail addresses: zhongshiwang@ciomp.ac.cn (Z. Wang), xur@ciomp.ac.cn (R. Xu), wangln@cust.edu.cn (L. Wang), d.tian@ciomp.ac.cn (D. Tian).

https://doi.org/10.1016/j.isatra.2021.12.001
0019-0578/

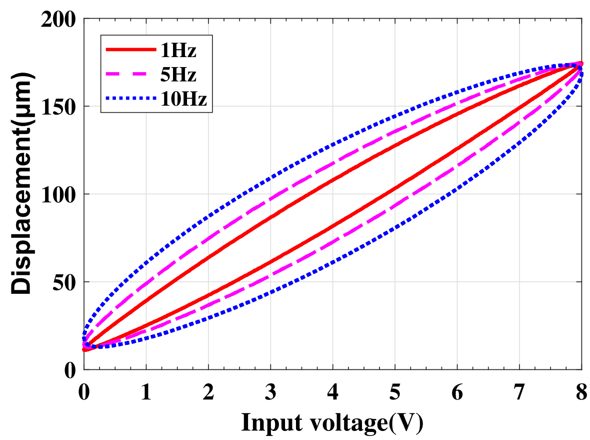

Fig. 1. Dynamic rate-dependent hysteresis characteristics.

and disturbance observer techniques [17,18]. Ming et al. developed a composite model predictive control with feedforward hysteresis compensation based on an inverse multiplicative structure. Their results show that its feedforward control enables it to enhance the positioning performance of the piezo-actuated stages [19]. Al Janaideh et al. applied the Prandtl–Ishlinskii feedforward technique to construct an H-infinity feedback control from the feedforward controlled actuator, which demonstrates the efficiency of the calculated controller [20]. However, the system is affected by external disturbances and uncertainty in the model parameters in addition to the internal dynamic hysteresis characteristic. Sliding mode control (SMC) provides an alternative way to deal with these issues and has been widely used to remove the disturbances for tracking control in piezoelectric systems [21,22]. However, a limitation of this approach is the existence of the switching strategy. To reduce chattering, it has been reported in [23] that an adaptive sliding mode controller with a proportional–derivative sliding surface improves performance in simulations. Xu presented the precision motion control of a piezoelectric nanopositioning stage using a scheme consisting of an adaptive sliding mode control with uncertainty and disturbance estimation [24], which has been proved in theory under Lyapunov stability.

Compared with classical stability, the main feature of finite-time control is that the state variables in dynamic systems converge to the equilibrium point in finite time and remain constant thereafter [25]. Finite-time stability can obtain fast, transient, and highly accurate performance [26]. Plestan et al. proposed a adaptive-gain sliding mode controller that is robust to uncertainties and disturbances [27]. In order to achieve the best dynamic performance, a dynamic hysteresis compensation method was developed by using a robust adaptive integral sliding mode controller, and the positioning error can converge to zero in finite time [28]. Xu proposed an adaptive integral terminal sliding-mode third-order finite-time control strategy specifically for motion tracking control in the piezo-actuated system [29]. However, few existing sliding mode controls for solving piezoelectric problems use finite time theory, which is not conducive to the application of piezo-actuated stages in practical engineering. Moreover, there is a lack of mature literature on the implementation of adaptive finite-time sliding mode control in embedded microprocessors.

Based on the above observation, this paper proposes a finite-time adaptive sliding mode control (FASMC) method with a PID sliding surface. The aim is to address dynamic hysteresis nonlinearities and uncertainty in the model parameters. Compared with current research achievements, the major contribution of this study is the design and implementation of a novel FASMC strategy.

(a) To improve the robustness and reduce chattering of the sliding mode controller, an adaptive switching-gain is added to the sliding mode controller with a PID sliding surface. Without knowing in advance the upper bound of the uncertainties, the adaptive switching-gain is dynamically tuned to ensure the sliding mode is established. Then, the gain is adjusted to obtain a value that is "sufficient" to eliminate the perturbations and uncertainties.
(b) To demonstrate its excellent tracking performance and robustness, the finite-time convergence conditions were analyzed, and the FASMC method was implemented in real time on an ARM microprocessor.

The remaining sections of this paper are organized as follows. Section 2 describes how the piezo-actuated stage is modeled by the combination of Bouc–Wen model and second-order differential function. In Section 3, the design process of the adaptive switching-gain sliding mode controller is presented and the finite-time convergence condition is demonstrated. Section 4 describes the model identification and experimental results. Finally, the conclusions of this study are presented in Section 5.

2. Dynamic hysteresis modeling

A piezoelectric stage is a complex motion system that can be divided into a linear part and a hysteresis nonlinear part [10].

(1) *Linear model.* Piezo-actuated stages often use a flexure-hinge-guided mechanism to provide motion through elastic deformations [30]. This monolithic design has no sliding parts, thus avoiding backlash and friction nonlinear characteristics, which makes the model closer to a second-order linear system. The linear part can be described by a general dynamic model that includes the electrical and mechanical modeling and is represented by the following second-order differential equation [7]:

$$m\ddot{x}(t) + b_s\dot{x}(t) + k_s x(t) = k_{em}(k_{amp}u(t) - h(t)), \tag{1}$$

where m, b_s, and k_s are the equivalent parameters of mass, damping, and stiffness, respectively; $x(t)$ is the output displacement of the piezo-actuated stage; k_{em} is an electromechanical transducer coefficient for describing the piezoelectric effect; k_{amp} is the gain of the driving amplifier; $u(t)$ is the control voltage for the driving amplifier; and $h(t)$ represents the voltage due to the hysteresis effect.

(2) *Hysteresis nonlinear model.* Among the differential-equation-based models, the Bouc–Wen model is the most common and suitable for our study. Thus, the hysteresis nonlinear model of a piezo-actuated stage can be described by the following differential equation:

$$\dot{h}(t) = \alpha\dot{u}(t) - \beta|\dot{u}(t)|h(t) - \gamma\dot{u}(t)|h(t)|, \tag{2}$$

where $\dot{h}(t)$ and $\dot{u}(t)$ denote the derivative of the voltage affected by hysteresis and the input control voltage, respectively. The magnitude and shape of the hysteresis loop is determined by three parameters: α, β, and γ.

To facilitate the control design, a more general form is given by combining Eqs. (1) and (2) as

$$\begin{cases} \ddot{x}(t) = a_0\dot{x}(t) + a_1 x(t) + a_2(u(t) + \Delta(t)) + a_3 h(t) \\ \dot{h}(t) = \alpha\dot{u} - \beta|\dot{u}|h(t) - \gamma\dot{u}|h(t)| \end{cases}, \tag{3}$$

where $a_0 = -\frac{b_s}{m} < 0$, $a_1 = -\frac{k_s}{m} < 0$, $a_2 = \frac{k_{em}k_{amp}}{m} > 0$, and $a_3 = -\frac{k_{em}}{m} < 0$. Further, $\Delta(t)$ represents an equivalent unstructured uncertainty that includes external disturbances and the uncertainty of the model parameters.

This model divides the piezo-actuated stage system into linear and nonlinear parts, representing the dynamic and hysteresis characteristics respectively. Since it is based on differential equations, it has the advantage of clear physical meanings for the parameters, simple controller design, and easy parameter identification.

3. Controller design

The most important task of controller design based on the dynamic hysteresis model (Eq. (3)) is to develop an effective strategy for achieving high-precision command tracking control while compensating for the unstructured uncertainty.

3.1. Sliding mode controller with PID surface

The SMC strategy is a common method for making the output of the nonlinear system track the command signal [31]. To design a SMC law to attenuate the hysteresis of the piezo-actuated stage, the displacement error is defined as

$$e(t) = x(t) - x_d(t), \tag{4}$$

where $x_d(t)$ is the desired output displacement of $x(t)$. The first- and second-order derivatives are easily obtained as

$$\dot{e}(t) = \dot{x}(t) - \dot{x}_d(t) \quad \text{and} \quad \ddot{e}(t) = \ddot{x}(t) - \ddot{x}_d(t). \tag{5}$$

Compared with the traditional sliding mode surface, i.e., the proportional–derivative surface, an integral term is used to improve the transient response and reduce the steady-state error in the sliding surface [32,33]. Then, a PID sliding mode surface is defined as

$$s(t) = k_{sp}e(t) + k_{si}\int_0^t e(\tau)d\tau + k_{sd}\dot{e}(t), \tag{6}$$

where k_{sp}, k_{si}, and k_{sd} are the proportional, integral, and derivative parameters of the sliding mode surface, respectively.

For the model (3), the sliding mode controller is designed in two parts as follows:

$$u(t) = u_{eq}(t) + u_n(t), \tag{7}$$

where

$$\begin{aligned} u_{eq}(t) =& \frac{1}{a_2}[\ddot{x}_d(t) - a_0\dot{x}(t) - a_1x(t) - a_3h(t) \\ & - \frac{k_{sp}}{k_{sd}}\dot{e}(t) - \frac{k_{si}}{k_{sd}}e(t)], \end{aligned} \tag{8}$$

$$u_n(t) = -k_{smc}sgn(s(t)). \tag{9}$$

Here, k_{smc} is the switching gain of the sliding mode controller and $sgn()$ represents a symbolic function.

Theorem 1. *If the parameters of the model (3) are known constants, and the state variable $\Delta(t)$ is bounded by D, then, using the PID sliding mode surface (6) and the sliding mode control law (7), the closed-loop system is asymptotically stable when the switching gain k_{smc} is selected as*

$$k_{smc} > D. \tag{10}$$

Proof. Based on the model (3), the time derivative of $s(t)$ in Eq. (6) is derived as follows:

$$\begin{aligned} \dot{s}(t) &= k_{sp}\dot{e}(t) + k_{si}e(t) + k_{sd}\ddot{e}(t) \\ &= k_{sp}\dot{e}(t) + k_{si}e(t) + k_{sd}(\ddot{x}(t) - \ddot{x}_d(t)) \\ &= k_{sp}\dot{e}(t) + k_{si}e(t) + k_{sd}[a_0\dot{x}(t) + a_1x(t) \\ &\quad + a_2(u(t) + \Delta(t)) + a_3h(t) - \ddot{x}_d(t)]. \end{aligned} \tag{11}$$

Substituting Eq. (7) into Eq. (11) yields

$$\dot{s}(t) = a_2k_{sd}[\Delta(t) - k_{smc}sgn(s(t))]. \tag{12}$$

The Lyapunov function candidate is considered as

$$V(t) = \frac{1}{2}s^2(t). \tag{13}$$

Then, the time derivative of $V(t)$ is obtained as

$$\dot{V}(t) = s(t)\dot{s}(t). \tag{14}$$

Substituting Eq. (11) into $\dot{V}(t)$ yields

$$\begin{aligned} \dot{V}(t) &= a_2k_{sd}[\Delta(t)s(t) - k_{smc}sgn(s(t))s(t)] \\ &= a_2k_{sd}[\Delta(t)s(t) - k_{smc}|s(t)|]. \end{aligned} \tag{15}$$

If $\Delta(t)$ is bounded by

$$|\Delta(t)| \le D, \tag{16}$$

where D is the upper bound of the equivalent unstructured uncertainty, then

$$\begin{aligned} \dot{V}(t) &\le a_2k_{sd}[|\Delta(t)||s(t)| - k_{smc}|s(t)|] \\ &\le a_2k_{sd}[D|s(t)| - k_{smc}|s(t)|] \\ &= a_2k_{sd}(D - k_{smc})|s(t)|. \end{aligned} \tag{17}$$

Here, because parameters a_2 and k_{sd} are positive, it can be easily obtained that k_{smc} must be chosen to be larger than D so that the derivative of the Lyapunov function becomes negative definite. Thus, the system is asymptotically stable under this condition, which allows the state to reach the sliding surface $s = 0$ [26]. □

Remark 1. Eq. (17) implies that the system states will not leave the sliding surface after reaching it, due to the negative part $\dot{V}(t)$. Based on the definition of the PID sliding surface, the parameters should be selected so that the characteristic polynomial $k_{sd}s^2 + k_{si}s + k_{sp} = 0$ is strictly Hurwitz, i.e., a polynomial with roots located strictly in the left half of the complex plane. This condition ensures the tracking error satisfies $\lim_{t\to\infty} e(t) = 0$ and $\lim_{t\to\infty}\dot{e}(t) = 0$ and that $x \to x_d$ and $\dot{x} \to \dot{x}_d$ as $t \to \infty$. Therefore, the SMC with a PID surface guarantees a zero steady-state tracking error.

Remark 2. The first- and second-order derivative of the desired displacement $\dot{x}_d(t), \ddot{x}_d(t)$ are required to obtain the controller (7). In practical application, the desired displacement command is often predefined. Hence, it is reasonable to calculate the controller (7) from $\dot{x}_d(t)$ and $\ddot{x}_d(t)$. For the derivative of the displacement $\dot{x}(t)$ in the controller (7), a lowpass filter is typically used to remove the sensor noise because displacement $x(t)$ is obtained by the sensor.

3.2. Finite-time adaptive switching-gain sliding mode control

In practical application, on the one hand, the model parameters identified offline include some uncertainty. To ensure stability, the switching gain should be improved. However, excessive switching gain can result in the system chattering. On the other hand, the equivalent unstructured uncertainty changes with respect to the environment and command signal. The equivalent unstructured uncertainty considered in $\Delta(t)$ is a variable state parameter. The fixed switching gain of the sliding mode controller (7) will lead to poor tracking performance and robustness. To improve this, an adaptive switching part is added to the sliding mode controller (7). This adaptive switching-gain is designed to resist the uncertainty in the model parameters and sudden external disturbances. Because the new adaptive term is adjusted online, this method can compensate for the shortcomings of the SMC method and achieve highly accurate tracking control of a piezo-actuated stage.

The control law (7) is rewritten as

$$\begin{aligned} u(t) =& \frac{1}{a_2}[\ddot{x}_d(t) - a_0\dot{x}(t) - a_1 x(t) - a_3 h(t)] \\ &- \frac{k_{sp}}{a_2 k_{sd}}\dot{e}(t) - \frac{k_{si}}{a_2 k_{sd}}e(t) \\ &- k_{smc}sgn(s(t)) - \hat{\eta}(t)sgn(s(t)), \end{aligned} \tag{18}$$

where $\hat{\eta}(t)$ is the adaptive switching gain and satisfies the adaptive rule

$$\dot{\hat{\eta}}(t) = -k_{ap}\hat{\eta}(t) + |s(t)|, \tag{19}$$

where k_{ap} is a positive constant that determines the convergence rate of the adaptive switching gain exponentially.

Theorem 2. *If the parameters of the model (3) are known constants and the state variable $\Delta(t)$ is bounded, then, using the adaptive sliding mode control law (18) and the adaptive rule (19), the closed-loop system has semi-global practical finite-time stability.*

Proof. We choose a new Lyapunov function $V_2(t)$,

$$V_2(t) = \frac{1}{2}s^2(t) + \frac{a_2}{2}\tilde{\eta}^2(t), \tag{20}$$

where $\tilde{\eta}(t) = D - \hat{\eta}(t)$. (To simplify the writing, the following proof omits (t).) Then, the first derivative of the Lyapunov function is

$$\dot{V}_2 = s\dot{s} + a_2\tilde{\eta}\dot{\tilde{\eta}}. \tag{21}$$

Substituting Eq. (11) into the above equation yields

$$\begin{aligned} \dot{V}_2 &= s[k_{sp}\dot{e} + k_{si}e + k_{sd}(\ddot{x} - \ddot{x}_d)] + a_2\tilde{\eta}\dot{\tilde{\eta}} \\ &= a_2 k_{sd}[\Delta \cdot s - (k_{smc} + \hat{\eta})|s|] + a_2\tilde{\eta}\dot{\tilde{\eta}}. \end{aligned} \tag{22}$$

Based on Eq. (18), the adaptive sliding mode control law is related to the ratios $\frac{k_{sp}}{k_{sd}}$ and $\frac{k_{si}}{k_{sd}}$. Thus, letting $k_{sd} = 1$, Eq. (22) can be simplified to

$$\begin{aligned} \dot{V}_2 &= a_2(\Delta \cdot s - k_{smc}|s| - \hat{\eta}|s| + \tilde{\eta}\dot{\tilde{\eta}}) \\ &\le a_2(D|s| - \hat{\eta}|s| - k_{smc}|s| + \tilde{\eta}\dot{\tilde{\eta}}) \\ &= a_2(\tilde{\eta}|s| - k_{smc}|s| + \tilde{\eta}\dot{\tilde{\eta}}). \end{aligned} \tag{23}$$

According to $\dot{\tilde{\eta}} = -\dot{\hat{\eta}}$, Eq. (23) is

$$\begin{aligned} \dot{V}_2 &\le a_2(\tilde{\eta}|s| - k_{smc}|s| - \tilde{\eta}(-k_{ap}\hat{\eta} + |s|)) \\ &= a_2(-k_{smc}|s| + k_{ap}\tilde{\eta}\hat{\eta}) \\ &= a_2(k_{ap}\tilde{\eta}(D - \tilde{\eta}) - k_{smc}|s|) \\ &= a_2(k_{ap}D\tilde{\eta} - k_{ap}\tilde{\eta}^2 - k_{smc}|s|) \\ &\le a_2(k_{ap}(\frac{D^2 + \tilde{\eta}^2}{2}) - k_{ap}\tilde{\eta}^2 - k_{smc}|s|) \\ &= a_2(\frac{k_{ap}}{2}D^2 - \frac{k_{ap}}{2}\tilde{\eta}^2 - k_{smc}|s|). \end{aligned} \tag{24}$$

Substituting $\frac{k_{ap}}{2}\tilde{\eta} - \frac{k_{ap}}{2}\tilde{\eta}$ into Eq. (24) yields

$$\dot{V}_2 \le a_2(\frac{k_{ap}}{2}D^2 + \frac{k_{ap}}{2}\tilde{\eta} - \frac{k_{ap}}{2}\tilde{\eta} - \frac{k_{ap}}{2}\tilde{\eta}^2 - k_{smc}|s|), \tag{25}$$

where

$$\begin{aligned} \frac{k_{ap}}{2}D^2 + \frac{k_{ap}}{2}\tilde{\eta} - \frac{k_{ap}}{2}\tilde{\eta}^2 &= \frac{k_{ap}}{2}(D^2 + \frac{1}{4} - \frac{1}{4} + \tilde{\eta} - \tilde{\eta}^2) \\ &= \frac{k_{ap}}{2}(D^2 + \frac{1}{4} - (\frac{1}{2} - \tilde{\eta})^2) \\ &\le \frac{k_{ap}}{2}(D^2 + \frac{1}{4}). \end{aligned} \tag{26}$$

Thus, $\frac{k_{ap}}{2}D^2 + \frac{k_{ap}}{2}\tilde{\eta} - \frac{k_{ap}}{2}\tilde{\eta}^2$ has an upper bound ς_0 as follows:

$$\varsigma_0 = \frac{k_{ap} + 4k_{ap}D^2}{8}. \tag{27}$$

Eq. (25) is simplified as

$$\begin{aligned} \dot{V}_2 &\le a_2(\varsigma_0 - \frac{k_{ap}}{2}\tilde{\eta} - k_{smc}|s|) \\ &= -a_2(\frac{k_{ap}}{2}\tilde{\eta} + k_{smc}|s|) + a_2\varsigma_0 \\ &\le -a_2\min\{\frac{k_{ap}}{2}, k_{smc}\}(\tilde{\eta} + |s|) + a_2\varsigma_0. \end{aligned} \tag{28}$$

Moreover, because

$$\begin{aligned} V_2^{0.5} &= (\frac{1}{2}s^2 + \frac{a_2}{2}\tilde{\eta}^2)^{\frac{1}{2}} \\ &\le \frac{1}{\sqrt{2}}|s| + \sqrt{\frac{a_2}{2}}\tilde{\eta} \\ &\le \max\{\frac{1}{\sqrt{2}}, \sqrt{\frac{a_2}{2}}\}(\tilde{\eta} + |s|). \end{aligned} \tag{29}$$

Combining inequality (28), we can obtain

$$\dot{V}_2 \le -\frac{a_2\min\{\frac{k_{ap}}{2}, k_{smc}\}}{\max\{\frac{1}{\sqrt{2}}, \sqrt{\frac{a_2}{2}}\}} \cdot V_2^{0.5} + a_2\varsigma_0. \tag{30}$$

Let $\nu = \frac{a_2\min\{\frac{k_{ap}}{2}, k_{smc}\}}{\max\{\frac{1}{\sqrt{2}}, \sqrt{\frac{a_2}{2}}\}}$. Then, we have

$$T_r \le \frac{2V_2^{0.5}(0)}{\kappa\theta_0}, \tag{31}$$

where

$$\kappa = \frac{(1 - \theta_0)\nu^2 V_2^{0.5}(0)}{(1 - \theta_0)\nu V_2^{0.5}(0) - a_2\varsigma_0}. \tag{32}$$

Here, $V_2(0)$ is the initial value of the Lyapunov function and θ_0 is a scalar from 0 to 1. The closed-loop system has semi-global practical finite-time stability and tracking error $e(t)$ converges to a small neighborhood around the origin in finite time T_r [25]. □

4. Experiment

In this section, the model identification and verification are first presented. To evaluate the effectiveness of FASMC, an experimental system was set up to compare FASMC with PID control and SMC, and the results are described.

4.1. Experimental setup

The experimental system includes a piezo-actuated stage, piezoelectric driving module (PDM), power supply, computer, and ARM microprocessor, as illustrated in Fig. 2.

The piezo-actuated stage is a P-542.2 (PI, Germany), and the PDM is an E-509.X3-503.00 (PI, Germany). The stroke of the piezo-actuated stage is 0∼200 μm. Switching power is used for the power supply of the ARM-based control system, and 28 VDC is provided. The experiment was carried out on an STM32F407 microprocessor, which is an ARM microprocessor with a 32-bit Cortex-M4 CPU and floating point unit. Its frequency can reach 168 MHz, which is a guarantee of high computation. The sampling time is set to 0.0002 s. ARM realizes real-time debugging through ST-LINK and communicates with the computer through an RS422-USB data line. The control algorithm was implemented in ARM. The control voltage is calculated and sent to PDM through the digital–analog converter. The PDM can provide a high voltage drive signal. Simultaneously, the feedback signals of strain gauge sensor are collected and sent to the ARM through an analog–digital converter.

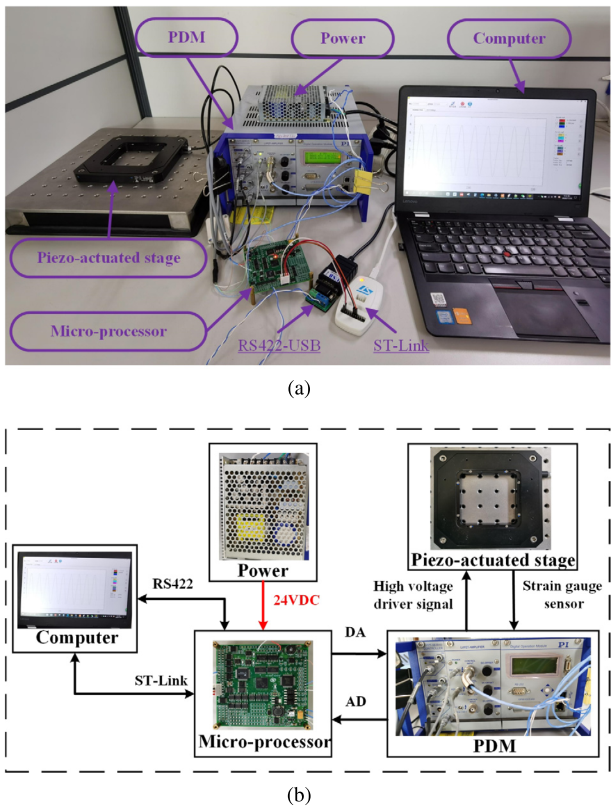

Fig. 2. ARM-based control system. (**a**) Experimental setup. (**b**) Control system structure block diagram.

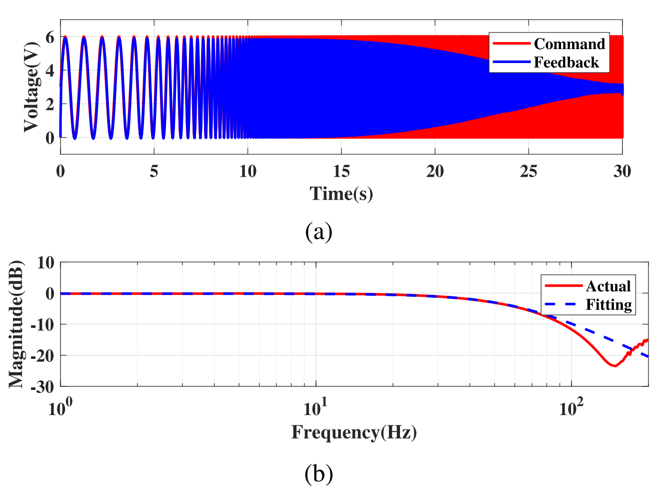

Fig. 3. Estimation results for the linear model. (**a**) Command and feedback signals. (**b**) Magnitude and frequency.

4.2. Model identification and validation

4.2.1. Linear model identification

The sinusoidal signal generated by the ARM microprocessor was used to identify the model of the linear part. Its amplitude was set to 6 V, which is also typically used in practice, and the frequency was gradually increased from 1 Hz to 150 Hz. The control and feedback voltage signals were used to estimate the transfer function of the linear part in Fig. 3.

It is observed that the magnitude of feedback signal decreases with the increase of frequency in Fig. 3(a). According to the model (3), a second-order transfer function is used to fit the magnitude–frequency curve in Fig. 3(b). The transfer function is estimated by the least squares method as follows:

$$G(s) = \frac{0.981 \times 400^2}{s^2 + 2 \times 0.85 \times 400s + 400^2}. \tag{33}$$

According to the estimated results in Eq. (33), we obtain the following model parameters: $a_0 = -680$, $a_1 = -160,000$, and $a_3 = -156,960$. Parameter a_2 contains not only the gain of the linear part but also the gain of the nonlinear part. Thus, the value of a_2 is given later.

Table 1
Parameter settings of the bat-inspired optimization algorithm.

Parameters	Values
Number of bats	50
Loudness	0.25
Pulse rates	0.35
Frequency range	[0,3]
Number of iterations	1000
Parameters for loudness update	0.05
Parameters for pulse rates update	0.95

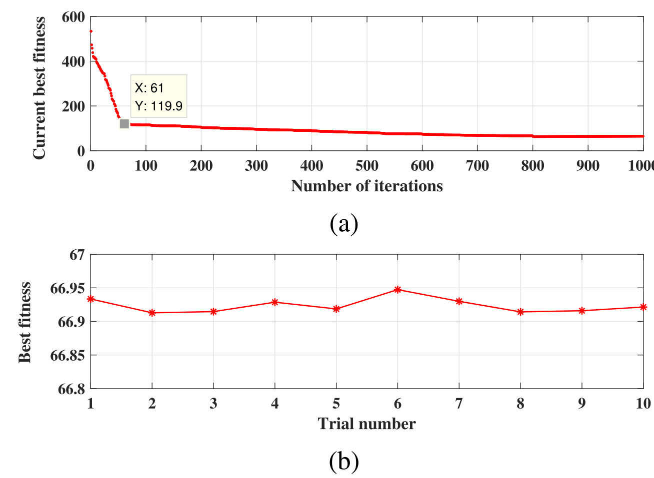

Fig. 4. Validation of the bat-inspired optimization algorithm. (**a**) Convergence; (**b**) Repeatability.

4.2.2. Nonlinear model identification based on the bat-inspired optimization algorithm

The nonlinear model was identified using the bat-inspired optimization algorithm [34]. First, some parameters in the bat-inspired algorithm that need to be determined are available. Through trial and error, the initial values for the parameters were selected and are listed in Table 1.

Using the parameters in Table 1, the convergence and repeatability results of the bat-inspired algorithm were verified by the current best fitness and the global best fitness. The current value of the best fitness with respect to the number of iterations is shown in Fig. 4(a), and the global best fitness values of 10 identification trials are shown in Fig. 4(b).

From Fig. 4, it is clear that the bat-inspired optimization algorithm can quickly converge to a better fitness value from the initial state. In addition, the global best fitness of the algorithm has good repeatability.

The sinusoidal signal with an amplitude of 8 V and frequency of 1 Hz was generated to draw the hysteresis loop. Five periods of data were used for identification, and the results of the nonlinear and estimation models are shown in Fig. 5.

The model accuracy was quantitatively assessed on the basis of global goodness-of-fit measures: the maximum error (MAXE),

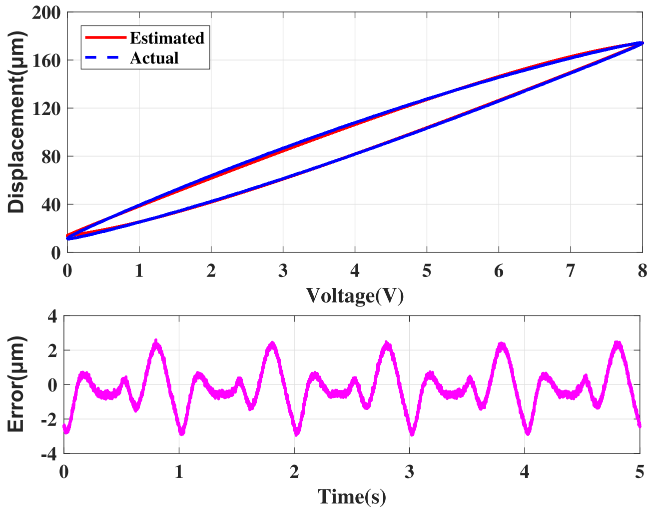

Fig. 5. Results of nonlinear model identification.

Table 2
Parameters of the dynamic hysteresis model.

Parameters	Values
a_0	−680
a_1	−160000
a_2	179750
a_3	−156960
α	0.3180
β	0.6662
γ	−0.0255

root-mean-squared error (RMSE), and maximum relative deviation (MRD), calculated as follows:

$$\mathrm{MAXE} = max|x_i - \hat{x}_i|, \tag{34}$$

$$\mathrm{RMSE} = \sqrt{\frac{1}{n}\sum_{i=1}^{n}|x_i - \hat{x}_i|^2}, \tag{35}$$

$$\mathrm{MRD} = \frac{\mathrm{MAXE}}{max(x_i)} \times 100\%, \tag{36}$$

where x_i is the actual measured displacement and $\hat{x}_i$ is the numerically estimated displacement by the model.

Fig. 5 shows that the model identification result of the bat-inspired optimization algorithm is very close to the actual system output. Quantitatively, the MAXE is 2.8013 μm, RMSE is 1.1694 μm, and MRD is 1.75%. Thus, the obtained model parameters capture the hysteresis characteristics of the piezo-actuated stage. All final parameter values of the dynamic hysteresis model are listed in Table 2.

4.2.3. Dynamic hysteresis model validation

To evaluate the accuracy of the dynamic hysteresis model (3), experiments were performed to compare the output of the estimated model and actual model based on the parameters obtained in Table 2. In the experiment, sinusoidal signals with frequencies of 1, 5, and 10 Hz were each given to the system. The outputs of the estimated and actual models are shown in Fig. 6. The deviation between the outputs of the estimated and actual models is given in Table 3.

The results show that the behavior of the estimated model is close to that of the actual system. At 1 Hz, the MAXE of the displacement is 2.8564μm, which includes the model parameter

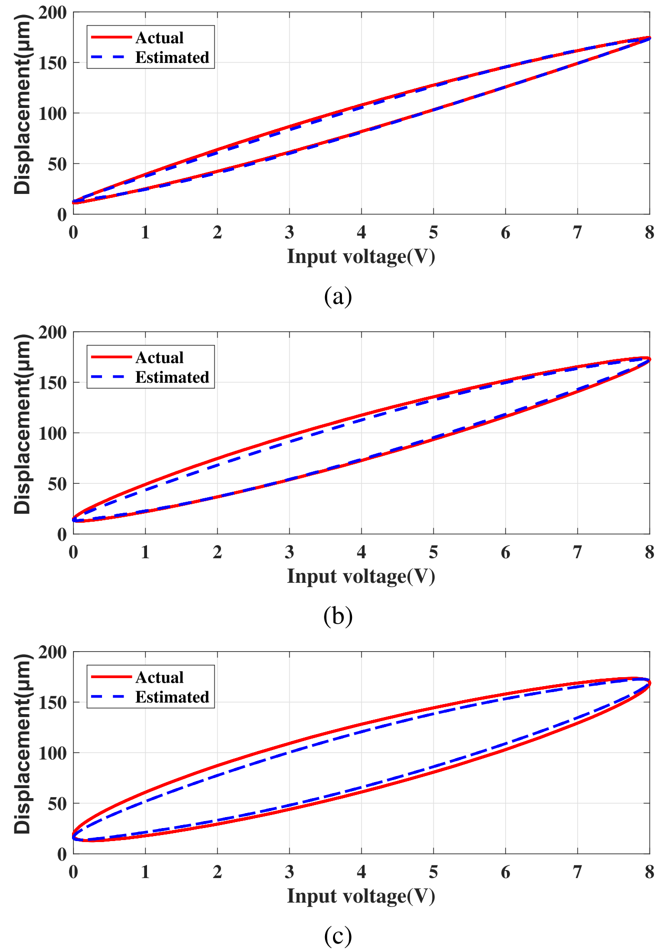

Fig. 6. Output of the estimated and actual models. (**a**) 1 Hz; (**b**) 5 Hz; (**c**) 10 Hz.

Table 3
Accuracy of the dynamic hysteresis model.

	1 Hz	5 Hz	10 Hz
MAXE (μm)	2.8564	5.6014	8.9169
RMSE (μm)	1.2413	2.7117	5.2760
MRD	1.79%	3.5%	5.57%

estimation error of 2.8013μm. Here, uncertainty in model parameters is the main source of error. As frequency increases, the nonlinear behavior becomes more severe. This will increase the uncertainty of the model parameters, leading to some difficulties in the controller design.

4.3. Experimental results

To demonstrate the effectiveness of the FASMC, sinusoidal and compound signals were used as the desired displacement command to implement tracking control experiments. Then, a 100 g load was added to the piezo-actuated stage to investigate the robustness of the FASMC. In the experiment, PID control and SMC were selected for comparison.

For fairness, a lowpass filter with a cutoff frequency of 400 rad/s was selected in the signal differential process of the three methods. To reduce the jitter of the sliding mode, we used the saturation function instead of the switching function, and the boundary layer of saturation function $sat(s)$ was set to 500 both in the SMC and FASMC. Considering the influence of these parameters on the performance of the controller, the values of the

Table 4
Control parameters of different controllers.

Controllers	Parameters
PID	$k_p = 0.15$, $k_i = 300$
SMC	$k_{sp} = 300$, $k_{si} = 300000$, $k_{sd} = 1$, $k_{smc} = 0.2$
FASMC	$k_{sp} = 300$, $k_{si} = 300000$, $k_{sd} = 1$, $k_{smc} = 0.2$, $k_{ap} = 4000$

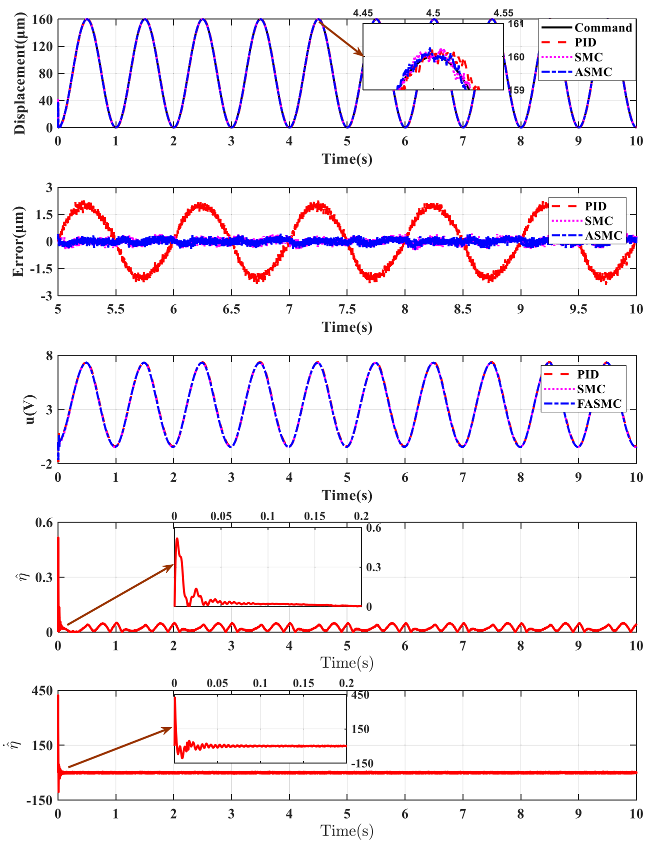

Fig. 7. Tracking results for 1 Hz sinusoidal signals.

parameters were adjusted experimentally. The parameter k_{smc} is positively related to the amplitude of the control signal, but increasing it also causes the signal to oscillate. Then, the values of k_{sp} and k_{si} are related to the rate at which the error converges to zero when the system reaches the sliding surface. After some trial-and-error preliminary experiments, we selected three groups of parameters with better performance, where FASMC was chosen to be the same as SMC for comparison, and they are listed in Table 4.

4.3.1. Tracking results for sinusoidal signals

An experimental test was conducted in which sinusoidal signals were tracked, where the reference command is described by $x_d(t) = 80\sin(2\pi ft - 0.5\pi) + 80$ μm; that is, the stroke was 160μm. The frequency was set to 1, 5, and 10 Hz. The tracking results are presented in Figs. 7∼ 9, where the displacement, the tracking error, and the control value $u(t)$ of The three methods are given, respectively. To evaluate the advantages of FASMC, the adaptive switching-gain $\hat{\eta}(t)$ and its derivative $\dot{\hat{\eta}}(t)$ are also shown.

A total of ten complete sinusoidal periods were selected to compare the displacement tracking results. It can be observed that the tracking performance of the PID control is the worst. In particular, as frequency increases, the PID control has a large tracking error. Both the SMC and FASMC methods can track a sinusoidal signal with higher accuracy than PID control.

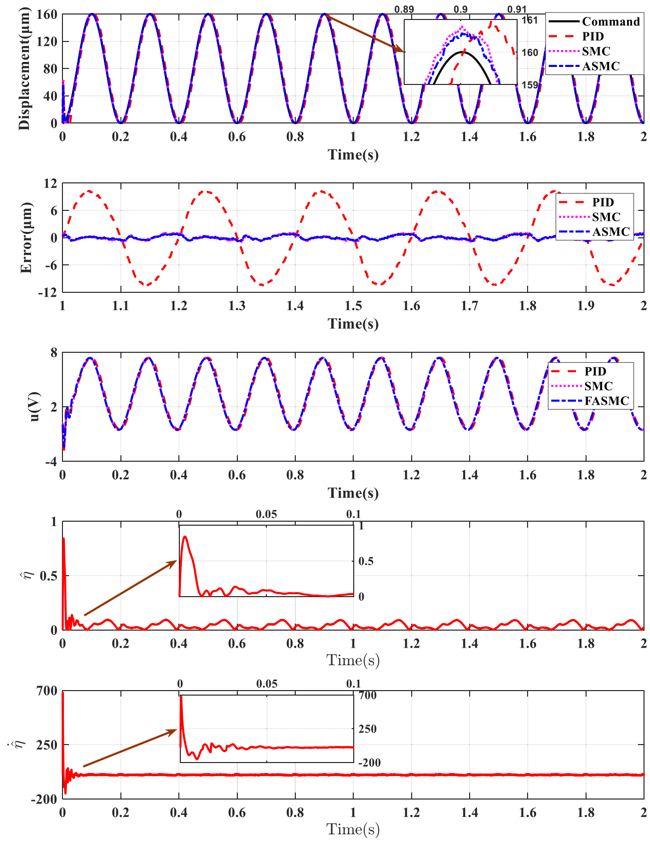

Fig. 8. Tracking results for 5 Hz sinusoidal signals.

Table 5
MAXE, RMSE, and MRD of sinusoidal signal tracking results with the three methods.

Command		PID	SMC	FASMC
1 Hz	MAXE (μm)	2.3850	0.5046	0.4499
	RMSE (μm)	1.4333	0.1351	0.1215
	MRD	1.49%	0.32%	0.28%
5 Hz	MAXE (μm)	10.5796	1.1305	0.9919
	RMSE (μm)	7.2945	0.5103	0.4144
	MRD	6.61%	0.71%	0.62%
10 Hz	MAXE (μm)	22.5370	3.7325	2.4282
	RMSE (μm)	14.9374	1.8875	1.3261
	MRD	14.09%	2.33%	1.52%

The unstructured uncertainty of the model increases as frequency increases. Figs. 7–9 clearly demonstrate that FASMC is capable of high precision sinusoidal command tracking, and the errors are guaranteed to converge to a small neighborhood around the equilibrium point in finite time. Also, all signals are guaranteed to have practical semi-global finite-time stability of the system even though the nonlinear systems are subject to the unstructured uncertainty. Further, the peak-to-peak value of the adaptive switching-gain gradually increases as the frequency increases. From this evidence, the advantages of the FASMC gradually appear. For quantitative comparison, the MAXE, RMSE, and MRD values of the three methods are listed in Table 5. Note that the error is calculated using the last five periods.

The MAXE, RMSE, and MRD of the SMC and FASMC methods are lower than those of the PID control method. The dynamic hysteresis model proposed in this study well describes the hysteresis nonlinear characteristics of the piezoelectric system. The

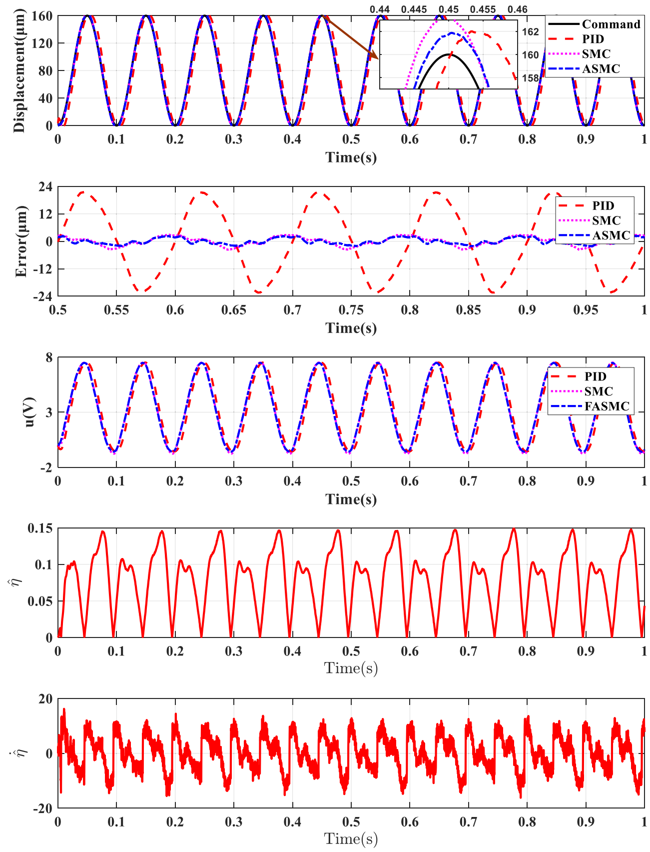

Fig. 9. Tracking results for 10 Hz sinusoidal signals.

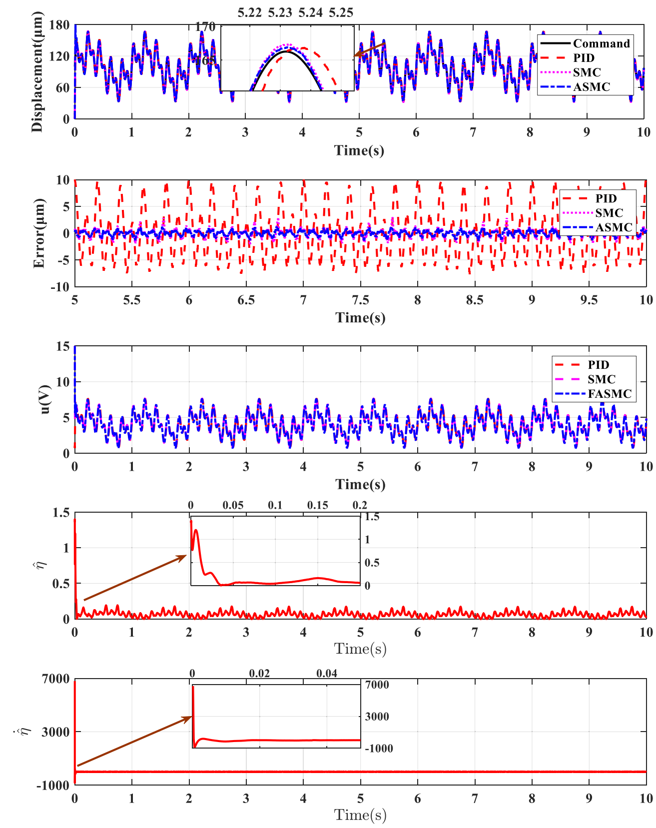

Fig. 10. Compound sinusoidal signal tracking results.

Table 6
MAXE, RMSE, and MRD of the compound signal tracking results with the three methods.

Command		PID	SMC	FASMC
Compound sin	MAXE (μm)	10.0063	2.7297	1.4142
	RMSE (μm)	4.8624	0.7751	0.4632
	MRD	6.02%	1.64%	0.85%
Compound tri	MAXE (μm)	0.8351	0.5717	0.4730
	RMSE (μm)	0.3288	0.1227	0.1041
	MRD	0.52%	0.36%	0.30%

controller based on the model can compensate for the rate-dependent characteristics of the piezo-actuated stage, and the switching gain can resist the equivalent unstructured uncertainty of the model. The FASMC method has the best sinusoidal tracking performance. Using the MRD as an example, the MRD of the three sinusoidal signals are 0.28%, 0.62%, and 1.52%, respectively, which are lower than the values of SMC by 12.5%, 12.7%, and 34.8%, respectively.

4.3.2. Tracking results for compound signals

To further evaluate the performance of the FASMC method, a multi-frequency and multi-amplitude sinusoidal signal was used for the tracking experiment. The signal is described by $x_d(t) = 28\sin(2\pi t) + 24\sin(10\pi t) + 20\sin(20\pi t) + 100\mu m$. Another multi-amplitude triangular signal was also used with the following amplitude changes: [0, 80, 60, 160, 100, 120, 0] μm. The compound signal tracking results, including the displacement, the tracking error, the control value $u(t)$, the adaptive switching-gain $\hat{\eta}$, and its derivative $\dot{\hat{\eta}}$ are depicted in Figs. 10 and 11. The performance indices were calculated for all three methods, and the results are compared in Table 6.

Similarly, as the command signal changes, the system state variables converge. Because of the better and faster action of the adaptive gain, the FASMC obtains the best tracking performance, with significant improvements in tracking accuracy and transient performance. In the tracking experiment of compound sinusoidal signal, the MAXE, RMSE, and MRD of FASMC decrease from the values of 2.7297 μm, 0.7751 μm, and 1.64% obtained by SMC to 1.4142 μm, 0.4632 μm and 0.85%, respectively. In the tracking experiment for the compound triangular signal, the MAXE, RMSE, and MRD of FASMC decrease from the values of 0.5717 μm, 0.1227 μm and 0.36% obtained by SMC to 0.4730 μm, 0.1041 μm and 0.30%, respectively. This result demonstrates that the dynamic hysteresis of the piezo-actuated stage has been successfully countered.

4.3.3. Results for robustness to unstructured uncertainty

In practical application, the dynamic hysteresis behavior of the piezo-actuated stage is related not only to the input command but also to the weight of load. The tracking experiments were implemented by mounting loads onto the piezo-actuated stage to evaluate the robustness of the FASMC to unstructured uncertainty. Because the previous experiments verified that the PID control has the worst performance, this experiment only compares SMC and FASMC. We mounted a 100 g load onto the piezo-actuated stage to carry out the motion tracking experiments with the FASMC method. The five input signals described above were again applied, and the tracking results with the load are compared in Table 7.

The results in Table 7 reveal that FASMC still has better tracking performance than SMC under the condition of a 100 g increase in the load. To compare the robustness of the FASMC, the percentage improvement in MRD from SMC to FASMC was calculated

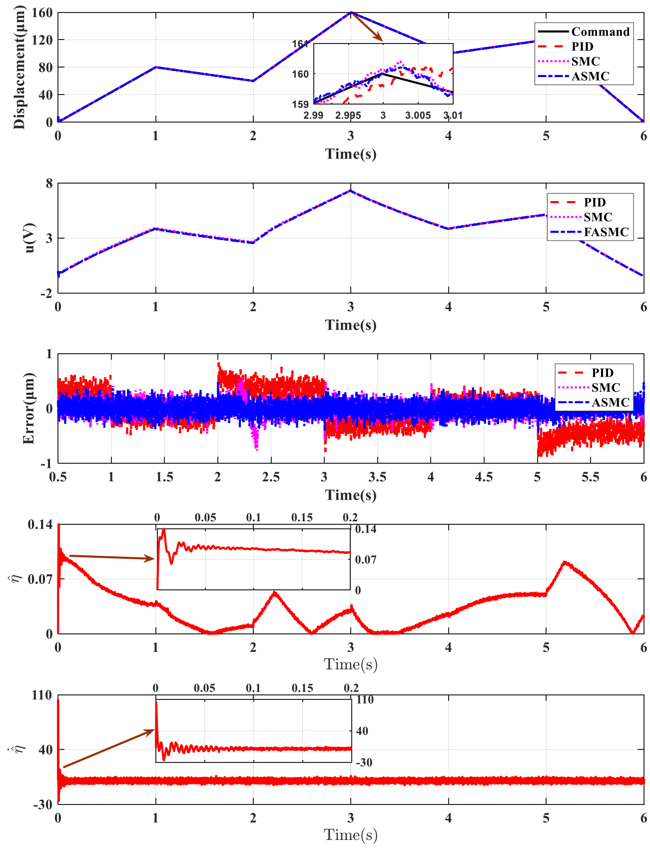

Fig. 11. Compound triangular signal tracking results.

Table 7
MAXE, RMSE, and MRD of tracking results with a 100-g load.

Command		SMC	FASMC
	MAXE (μm)	0.6003	0.5119
1 Hz	RMSE (μm)	0.1793	0.1384
	MRD	0.38%	0.32%
	MAXE (μm)	1.6119	1.1378
5 Hz	RMSE (μm)	0.7117	0.4895
	MRD	1.01%	0.71%
	MAXE (μm)	5.4611	2.9904
10 Hz	RMSE (μm)	2.7044	1.5328
	MRD	3.41%	1.87%
	MAXE (μm)	2.9940	1.5200
Compound sin	RMSE (μm)	0.7462	0.4972
	MRD	1.87%	0.91%
	MAXE (μm)	2.2443	0.5179
Compound tri	RMSE (μm)	0.5776	0.1143
	MRD	1.40%	0.32%

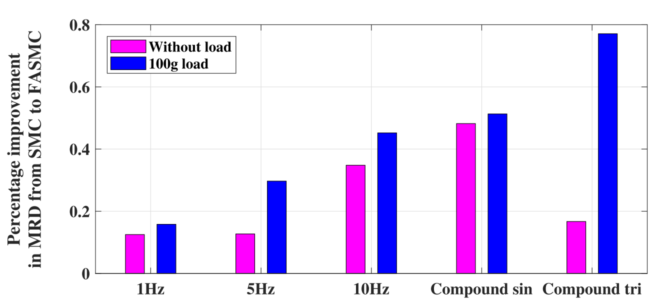

Fig. 12. Percentage improvement in MRD from SMC to FASMC.

both with no load and a 100-g load, and the results are shown in Fig. 12.

With a 100-g load, the percentage improvements in MRD from SMC to FASMC are 15.8%, 29.7%, 45.2%, 51.3%, and 77.1%, respectively, whereas the values are 12.5%, 12.7%, 34.8%, 48.2%, and 16.7% without a load. These results demonstrate that the FASMC has better robustness when the unstructured uncertainty increases.

5. Conclusion

This paper introduced a finite-time adaptive sliding mode control algorithm for high-precision tracking of a piezo-actuated stage system. The proposed FASMC method can adaptively capture the dynamic hysteresis characteristics and exhibits robustness against unstructured uncertainty.

When tracking a sinusoidal signal with a frequency of 10 Hz and amplitude of 160μm, the FASMC algorithm obtains the smallest tracking error, with an MRD of 1.52%, whereas the MRD of the SMC algorithm is 2.33%. The percentage improvement in MRD from SMC to FASMC is 34.8%. In addition, the MRD of FASMC and SMC are 1.87% and 3.41% after adding a 100-g load, respectively. The percentage improvement in MRD is 45.2%.

The results of the ARM-based experiments show that FASMC improves the tracking performance and robustness of the piezo-actuated stage system when compared with PID and SMC. Moreover, the dynamic hysteresis characteristic have been suppressed effectively, and this result provides a powerful reference for engineering application. In future research, we will investigate the application of the FASMC algorithm in the piezo-actuated stage when the control voltage is saturated.

CRediT authorship contribution statement

Zhongshi Wang: Conceptualization, Methodology, Validation, Software, Writing – original draft. **Rui Xu:** Formula analysis. **Lina Wang:** Data curation, Writing – review & editing. **Dapeng Tian:** Review, Supervision, Project administration.

Declaration of competing interest

The authors declare that they have no known competing financial interests or personal relationships that could have appeared to influence the work reported in this paper.

Acknowledgments

This paper is supported by National Science Foundation of China [Grant No. 62103396], Key Research Program of Frontier Science of Chinese Academy of Sciences [Grant No. DBS-LY-JSC044], and China Postdoctoral Science Foundation [Grant No. 2020TQ0350].

References

[1] Li Y, Xu Q. Adaptive sliding mode control with perturbation estimation and PID sliding surface for motion tracking of a piezo-driven micromanipulator. IEEE Trans Control Syst Technol 2010;18(4):798–810.
[2] Li H, Han K, Wang X, He S, Wu Q, et al. A compact and lightweight two-dimensional gimbal for inter-satellite laser communication applications. Opt Express 2019;27(17):24060–71.
[3] Li Q, Liu L, Ma X, Chen S, Yun H, et al. Development of multitarget acquisition, pointing, and tracking system for airborne laser communication. IEEE Trans Industr Inform 2019;15(3):1720–9.
[4] Lau JY, Liang W, Tan KK. Adaptive sliding mode enhanced disturbance observer-based control of surgical device. ISA Trans 2019;90:178–88.
[5] Wang G, Wang Y, Zhou H, Bai F, Chen G, et al. Comprehensive approach to modeling and identification of a two-axis piezoelectric fast steering mirror system based on multi-component analysis and synthesis. Mech Syst Signal Process 2019;127:50–67.

[6] Xiao S, Li Y. Modeling and high dynamic compensating the rate-dependent hysteresis of piezoelectric actuators via a novel modified inverse Preisach model. IEEE Trans Control Syst Technol 2013;21(5):1549–57.

[7] Gu G, Zhu L, Su C, Ding H. Motion control of piezoelectric positioning stages: modeling, controller design, and experimental evaluation. IEEE/ASME Trans Mechatron 2013;18(5):1459–71.

[8] Madadi E, Soeffker D. Model-free approaches applied to the control of nonlinear systems: a brief survey with special attention to intelligent PID iterative learning control. In: 8th ASME annual dynamic systems and control conference. Columbus; 2015. p. 1–8.

[9] Wang X, Lee KH, Fu DKC, Dong ZY, Wang K, et al. Experimental validation of robotassisted cardiovascular catheterization: model-based versus modelfree control. Int J Comput Assist Radiol Surg 2018;13(6):797–804.

[10] Gu G, Zhu L, Su C, Ding H, Fatikow S. Modeling and control of piezo-actuated nanopositioning stages: a survey. IEEE Trans Autom Sci Eng 2016;13(1):313–32.

[11] Li Z, Su C, Chai T. Compensation of hysteresis nonlinearity in magnetostrictive actuators with inverse multiplicative structure for preisach model. IEEE Trans Autom Sci Eng 2014;11(2):613–9.

[12] Xu R, Tian D, Zhou M. A rate-dependent KP modeling and direct compensation control technique for hysteresis in piezo-nanopositioning stages. J Intell Mater Syst Struct 2021;1–12.

[13] Janaideh MA, Xu R, Tan X. Adaptive estimation of play Radii for a Prandtl–Ishlinskii hysteresis operator. IEEE Trans Control Syst Technol 2021;29(6):2687–95.

[14] Ahmed K, Yan P, Li S. Duhem model-based hysteresis identification in piezo-actuated nano-stage using modified particle swarm optimization. Micromachines 2021;12(3):315.

[15] Tan Y, Li Y, Dong R, Chen X, He H. A nonsmooth kalman filter for state estimation of positioning stage based on Sandwich model with Backlash-like hysteresis. In: American conrtol conference. Boston, MA, USA; 2016. p. 661–666.

[16] Zaman M, Sikder U. Bouc-Wen hysteresis model identification using modified firefly algorithm. J Magn Magn Mater 2015;395:229–33.

[17] Al Janaideh M, Rakotondrabe M, Al-Darabsah I, Aljanaideh O. Internal model-based feedback control design for inversion-free feedforward rate-dependent hysteresis compensation of piezoelectric cantilever actuator. Control Eng Pract 2018;72:29–41.

[18] Nie Z, Ma Y, Liu R, Guo D. Improved disturbance rejection control for piezoelectric actuators based on combination of ESO and Q-filter. Electron Lett 2018;54(14):872–4.

[19] Ming M, Ling J, Feng Z, Xiao X. A model prediction control design for inverse multiplicative structure based feedforward hysteresis compensation of a piezo nanopositioning stage. Int J Precis Eng Manuf 2018;19(11):1699–708.

[20] Al Janaideh M, Rakotondrabe M, Aljanaideh O. Further results on hysteresis compensation of smart micropositioning systems with the inverse Prandtl–Ishlinskii compensator. IEEE Trans Control Syst Technol 2016;24(2):428–39.

[21] Gan M, Qiao Z, Li Y. Liding mode control with perturbation estimation and hysteresis compensator based on Bouc-Wen model in tackling fast-varying sinusoidal position control of a piezoelectric actuator. J Syst Sci Complex 2016;29(2):367–81.

[22] Xu R, Pan W, Wang Z, Tian D. High-precision tracking control of a piezoelectric micro-nano platform using sliding mode control with the fractional-order operator. Int J Precis Eng Manuf 2020;29(12):2277–86.

[23] Alem S, Izadi I, Sheikholeslam F. Adaptive sliding mode control of hysteresis in piezoelectric actuator. In: International federation of automatic control. Toulouse, France; 2017, p. 15574–9.

[24] Xu Q. Precision motion control of piezoelectric nanopositioning stage with chattering-free adaptive sliding mode control. IEEE Trans Autom Sci Eng 2017;14(1):238–48.

[25] Wang H, Chen B, Lin C, Sun Y, Wang F. Adaptive finite-time control for a class of uncertain high-order non-linear systems based on fuzzy approximation. IET Control Theory Appl 2017;11(5):677–84.

[26] Wang G, Xu Q. Adaptive terminal sliding mode control for motion tracking of a micropositioning system. Asian J Control 2018;20(3):1241–52.

[27] Plestan F, Shtessel Y, Bregeault V, Poznyak A. New methodologies for adaptive sliding mode control. Internat J Control 2010;83(9):1907–19.

[28] Zhang Y, Yan P. An adaptive integral sliding mode control approach for piezoelectric nano-manipulation with optimal transient performance. Mechatronics 2018;52:119–26.

[29] Xu Q. Adaptive integral terminal third-order finite-time sliding-mode strategy for robust nanopositioning control. IEEE Trans Ind Electron 2021;68(7):6161–70.

[30] Kiziroglou ME, Temelkuran B, Yeatman EM, Yang G. Micro motion amplification–a review. IEEE Access 2020;8:64037–55.

[31] Xu R, Zhang X, Guo H, Zhou M. Sliding mode tracking control with perturbation estimation for hysteresis nonlinearity of piezo-actuated stages. IEEE Access 2018;6:30617–29.

[32] Gu G, Li C, Zhu L, Fatikow S. Robust tracking of nanopositioning stages using sliding mode control with a PID sliding surface. In: IEEE/ASME International Conference on Advanced Intelligent Mechatronics . Besançon, France; 2014. p. 973–977.

[33] Fang J, Zhang L, Long Z, Wang M. Fuzzy adaptive sliding mode control for the precision position of piezo-actuated nano positioning stage. Int J Precis Eng Manuf 2018;19(10):1447–56.

[34] Yang XS. A new metaheuristic bat-inspired algorithm. In: Nature inspired cooperative strategies for optimization. 2010, p. 65–74.

Zhongshi Wang (zhongshiwang@ciomp.ac.cn) received the M.Eng. degree in control theory and control engineering with the College of Automation, Haerbin Engineering University, China, in 2014. He received the Ph.D. degree in mechatronic engineering from University of Chinese Academy of Sciences in 2021. He is currently an assistant researcher in the Key Laboratory of Airborne Optical Imaging and Measurement (AOIM), Changchun Institute of Optics, Fine Mechanics and Physics (CIOMP), Chinese Academy of Sciences (CAS), Changchun, China. His research interests include micro-nano control and motion control.

Rui Xu (xur@ciomp.ac.cn) received the Ph.D. degree in control theory and control engineering with the Department of Control Science and Engineering, Jilin University, Changchun, China, in 2019. From Sep. 2018 to Sep. 2019, he was an exchange PhD student with the Department of Electrical and Computer Engineering, Michigan State University, East Lansing, USA. Since 2020, he has been with the Key Laboratory of AOIM, CIOMP, CAS, Changchun, China. His current research interests include micro-nano drive control, motion control theory and optical imaging.

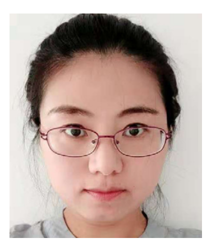

Lina Wang (wanglina18@mails.ucas.ac.cn) received the M.Eng. degree in control theory and control engineering with the College of Automation, Haerbin Engineering University, China, in 2014. He received the Ph.D. degree in mechatronic engineering from University of Chinese Academy of Sciences in 2021. She is currently a researcher in the College of Electro-Mechanical Engineering, Changchun University of Science and Technology, Changchun, China. Her research interests include feature detection and image registration.

Dapeng Tian (d.tian@ciomp.ac.cn) received the B.E. degree from Beijing Institute of Technology, Beijing, China, in 2007. He was then directly recommended to study at Beihang University, Beijing, where he received the Ph.D. degree in 2012. From 2009 to 2011, he was a Co-researcher with the Advanced Research Center, Keio University, Yokohama, Japan. Since 2012, he has been with the Key Laboratory of AOIM, CIOMP, CAS, Changchun, China, where he is currently a Full Professor. His current research interests include motion control theory and engineering, optical imaging, and bilateral control.